Control of the Shell Structural Properties and Cavity Diameter of Hollow Magnesium Fluoride Particles

Asep Bayu Dani Nandiyanto,[†,‡] Takashi Ogi,*,[†] and Kikuo Okuyama[†]

[†]Department of Chemical Engineering, Graduate School of Engineering, Hiroshima University, 1-4-1 Kagamiyama, Higashi Hiroshima, Hiroshima 739-8527, Japan

[‡]Departemen Kimia, Fakultas Pendidikan Matematika dan Ilmu Pengetahuan Alam, Universitas Pendidikan Indonesia, Jl. Dr. Setiabudhi No. 229, Bandung 40154, Indonesia
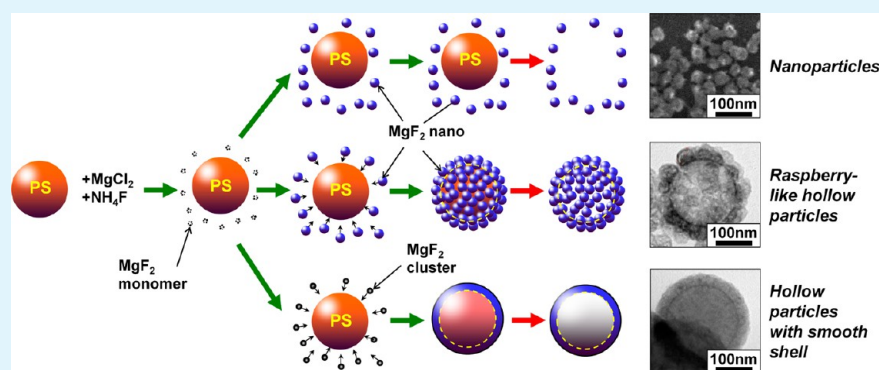
ABSTRACT: Control of the shell structural properties [i.e., thickness (8−25 nm) and morphology (dense and raspberry)] and cavity diameter (100−350 nm) of hollow particles was investigated experimentally, and the results were qualitatively explained based on the available theory. We found that the selective deposition size and formation of the shell component on the surface of a core template played important roles in controlling the structure of the resulting shell. To achieve the selective deposition size and formation of the shell component, various process parameters (i.e., reaction temperature and charge, size, and composition of the core template and shell components) were tested. Magnesium fluoride (MgF_2) and polystyrene spheres were used as models for shell and core components, respectively. MgF_2 was selected because, to the best of our knowledge, the current reported approaches to date were limited to synthesis of MgF_2 in film and particle forms only. Therefore, understanding how to control the formation of MgF_2 with various structures (both the thickness and morphology) is a prospective for advanced lens synthesis and applications.

KEYWORDS: core−shell, hollow structure, thin film, coating mechanism, ζ potential

1. INTRODUCTION

A material with hollow structures possesses excellent characteristics. Its excellent performance makes this material suitable for a wide range of applications, such as thermal insulators, optical devices, chromatography-related components, shields for enzymes and proteins, drug-delivery vehicles, dyes, inks, photonic crystals, artificial cells, waste treatment, and large biomolecular release systems.[1]

The most common strategy to synthesize hollow particles involves the pasting of the shell component on the surface of the core particle, followed by a core removal process.[2] In the synthesis procedure, the shell component can be from either nanoparticles or active chemical/reactants.[3] Despite the popularity of this method, the latter presents several limitations: (1) Current methods cannot be separated from the use of additives (e.g., polymers, surfactants, salts, acid) for pasting the shell component on the core surface. In turn, this additive can create unexpected shell structures and compromise the final product (because of incomplete additive removal).[4] (2) Information

relating to the synthesis of discrete functional hollow particles with controllable outer diameter, shell thickness, and shell morphology is nonexhaustive. (3) The influence of the core and shell charges on the coating process is not comprehensively addressed. In fact, this factor is important for the fabrication of hollow or porous materials with different hole configurations.[5] (4) The applicability of current synthesis strategies to create different hollow materials is limited. To date, hollow silica and titania entities have received the most attention, and only a few studies have successfully reported the synthesis of other materials. More specifically, there is no detailed information on the preparation of fluoride materials with hollow structures.

In our previous reports, we studied the synthesis of hollow and porous particles using a colloidal templating method in the liquid phase.[4−10] The effects of the physicochemical properties of the
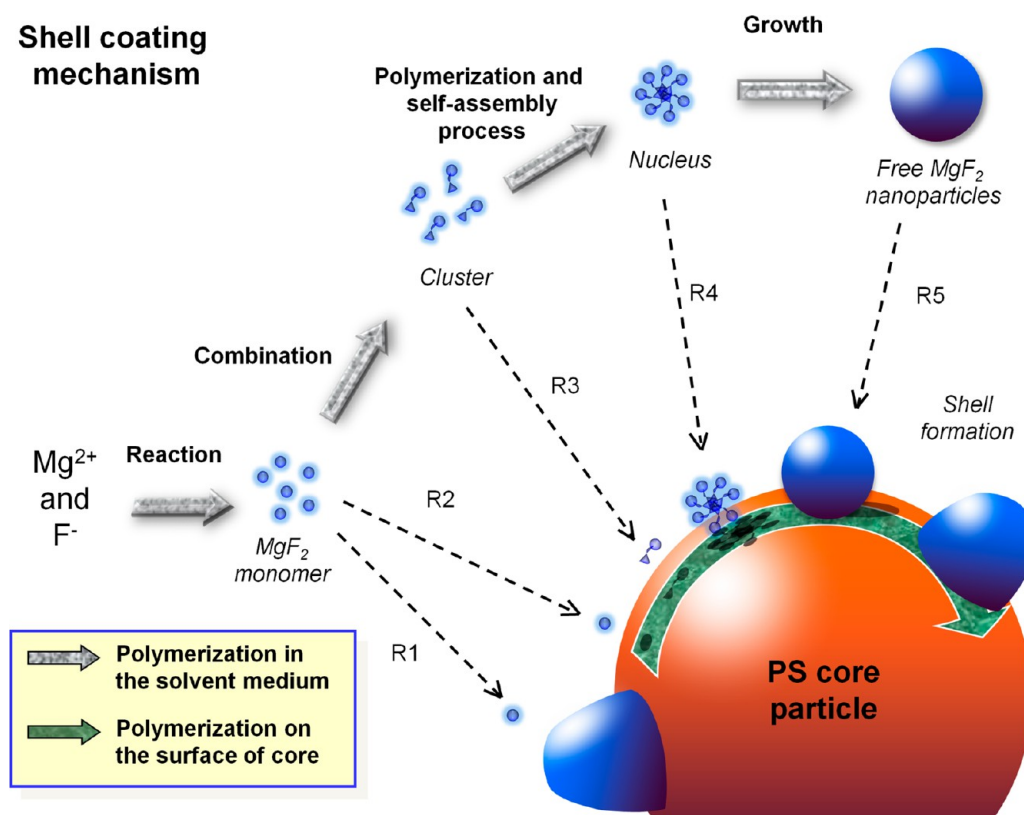
Figure 1. Schematic illustration of the formation of MgF_2 on the surface of the PS core.

core and shell components (i.e., surface charge, size, and composition) were examined. However, our previous studies are limited to the synthesis of silica only, and we did not discuss on how to control the shell morphology.

Here, we present a theoretical explanation for control of the shell structural properties [i.e., thickness (8−25 nm) and morphology (dense and raspberry)] and cavity diameter (100−350 nm) of hollow particles. The selective deposition size and formation of the shell component on the surface of a core template appear to have important effects on controlling the structure of the resulting shell. To achieve the selective deposition size and formation of the shell component, the reaction temperature and charge, size, and composition of the core template and shell components were tested.

In the experimental procedure, the hollow particles were synthesized by forming and growing the shell component on the surface of a colloidal core under additive-free conditions, followed by a core removal process. Magnesium fluoride (MgF_2) and polystyrene (PS) spheres were used as models for the shell and core components, respectively.

We selected MgF_2 as the main shell component because this material has excellent properties (e.g., low refractive index, corrosion resistance, thermal stability, and significant hardness), which is useful for a wide range of applications such as catalytic support, coating materials, and antireflective lenses.[9] Therefore, we believe that understanding how to tailor the formation of MgF_2 with various structures (both the thickness and morphology) is a prospective for advanced lens synthesis and applications because control of this structure has a correlation with controlling the optical properties,[11] such as the refractive index. However, the reported approaches to date were limited to the synthesis of MgF_2 in film[12−17] and particle[18−24] forms only. Although Grosso et al.[25] has reported the successful synthesis of hollow magnesium oxyfluoride

nanoparticles, there is no information about control of the cavity diameter and shell thickness, and their method is applicable only in the film form.

In addition, our method succeeded in pasting and forming a shell on the core surface under additive-free conditions only by modulating the surface charge of the core template, while current coating processes need the support of the additive.

2. HYPOTHETICAL FORMATION OF THE SHELL COMPONENT ON THE CORE SURFACE

Figure 1 shows a schematic illustration of the coating process in the liquid phase. In this model, PS spheres, magnesium chloride ($MgCl_2$), and ammonium fluoride (NH_4F) were used as the core, magnesium source, and fluoride source, respectively. In this approach, $MgCl_2$ and NH_4F quickly dissolve to form Mg^{2+} and F^- ions in solution, facilitating the formation of MgF_2 monomers, clusters, nuclei, and particles (as indicated by the gray arrows). To simplify the explanation, the formation and growth of MgF_2 molecular networks are herein termed "polymerization". The resulting MgF_2 then deposits onto the core surface. Several deposition mechanism routes are possible (as shown by the black and dashed arrows): diffusion−adsorption of MgF_2 monomers/oligomers on the PS core surface (routes R1 and R2), attraction and aggregation of MgF_2 clusters, nuclei, and nanoparticles to the PS core surface (routes R3−R5), and growth of the nuclei to form free MgF_2 nanoparticles. To proceed with growth and complete shell formation (as shown by the green arrow), the deposited MgF_2 reacts with the available monomer in solution (route R1).

On the basis of the proposed model, the two factors involved for successful coating are MgF_2 formation (including reactant interaction, reaction, nucleation, and growth processes, as

indicated by the gray arrows) and MgF_2 deposition (as shown by the black and dashed arrows). The MgF_2 formation process factor determines the size of the initial MgF_2 to be deposited, whereas the MgF_2 deposition process factor relates to the attraction mechanism between the MgF_2 component and PS surface.

The first factor (MgF_2 formation) can be predicted using conventional nucleation and growth theories, whereby the rate of MgF_2 formation is proportional to $\exp(-Q/RT)$, where R is the gas constant, T is the temperature, and Q is the free-energy change of the process.[26,27] The rate of shell formation is also influenced by the presence of reactants, catalysts, and additives.[28]

Relating to the second factor, the rate of shell deposition can be approximated by the particle kinetic aggregation phenomenon.[29] Assuming that the colloidal core and shell components are inelastic and irreversible, deposition of the shell component on the surface of a core can be approximated by

$$\frac{dN_m}{dt} \approx \frac{1}{2} \sum_{i+j=m} K_{ij}N_iN_j - \sum_j K_{mj}N_mN_j \tag{1}$$

where i and j are the colliding units (i.e., core and shell components), m is the number of aggregated units, N is the number of colliding units, and K_{ij} is the cohesion rate when unit i collides with unit j. The m value can be estimated from the number of MgF_2 formed from conversion of the magnesium and fluoride sources. The K_{ij} value can be estimated by

$$K_{ij} = 4\pi(R_{col,i} + R_{col,j})(D_i + D_j) + F \tag{2}$$

where R_{col} and D are the collision radius and diffusion coefficient of the unit, respectively, and F is the coefficient factor resulting from unit–unit interaction (attraction and repulsion of units), additive effects, and random-walk diffusion before both the units come into close proximity and stick together.

The above theoretical approximations suggest that, to get excellent shell formation under additive-free conditions, a smart strategy capable of controlling the interaction, reaction, and growth of MgF_2 on the surface of PS can be achieved by managing several synthesis parameters. The temperature and number of MgF_2 components (depending on the availability of the reactants) affect the MgF_2 formation process factor. The physicochemical properties of the PS core and MgF_2 components (i.e., surface charge, size, and composition) influence the MgF_2 deposition process factor. These parameters are essential to maintaining the selective deposition size and formation of MgF_2 on the PS core surface to afford hollow MgF_2 particles with a controllable shell structure.

3. EXPERIMENTAL SECTION

Hollow MgF_2 particles were synthesized using the following raw materials: surfactant-free PS sphere, $MgCl_2$ (Kanto Chemical Co. Inc., Japan), and NH_4F (Aldrich, USA). The surfactant-free PS spheres were synthesized by simple polymerization of a styrene monomer (Kanto Chemical Co. Inc., Japan) in aqueous solution, as detailed in our previous work.[8] Potassium persulfate (KPS; Aldrich, USA) or 2,2′-azobis(isobutyramidine) dihydrochloride (AIBA; Sigma-Aldrich, USA) was used as the initiator in the styrene polymerization process.

Typically, PS colloidal spheres were diluted in an aqueous solution; the resulting suspension was vigorously stirred and heated at a specific temperature for 30 min, affording a well-heated and homogeneous dispersion. After 30 min of stirring, $MgCl_2$ and NH_4F were added subsequently. This mixture is referred to as the precursor. The precursor was then mixed for another 1 h. Finally, the resulting solution was cooled to room temperature and purified via centrifugation at 15000 rpm for 30 min (washing with ethanol). The purified particles were dried and heated at 500 °C to remove the PS core. The $MgCl_2/NH_4F$ molar ratio was varied in the range of 1.0 and 5.50 at a constant PS concentration of 0.27 g L^{-1}. The reaction temperature was varied from 30 to 75 °C.

The size, morphology, and structure of the prepared particles were characterized by a scanning electron microscope (Hitachi S-5000, Hitachi, Japan, operating at 20 kV) and a transmission electron microscope (JEM-2010, JEOL Ltd., Japan, operating at 200 kV). Elemental and chemical compositions of the prepared particles were evaluated by an X-ray diffractometer (Rigaku Denki RINT 2000, using Cu Kα radiation) and a scanning transmission electron microscope equipped with an energy-dispersive X-ray (EDS) unit.

4. RESULTS AND DISCUSSION

4.1. Physicochemical Properties of the Prepared Particles.

The physicochemical properties of the prepared particles at different stages of the synthesis were examined. Figure 2a shows the scanning electron microscopy (SEM) image of the synthesized PS spheres. PS spheres were monodisperse in size and featured a smooth surface. The addition of magnesium and fluoride sources in the PS solution generated particles with a rough surface, as shown in Figure 2b. The size of the as-synthesized particles was similar to that of the initial PS spheres. Following heat treatment at 500 °C, both the outer shape and diameter of the particles remained unchanged (Figure 2c). Some crevasses or cracks were observed, indicating the hollow structure in the particle.

To confirm the structure inside the particles, transmission electron microscopy (TEM) analysis was conducted (Figure 2d–f). TEM images showed that the PS particles were dense and spherical (Figure 2d). TEM analysis of as-synthesized particles displayed a core–shell structure (Figure 2e), whereas that of particles following heat treatment at 500 °C featured a hollow structure (Figure 2f).

X-ray diffraction (XRD) patterns of the particles before and after heat treatment featured MgF_2 diffraction peaks (Figure 2g), which was confirmed by the Joint Committee on Powder Diffraction Standards (JCPDS) number 006-0290. EDS analysis also detected the presence of MgF_2 in the as-synthesized samples before and after heat treatment (Figure 2h).

Scanning transmission electron microscopy (STEM) results of the particles after heat treatment (shown in Figure 3a) were consistent with TEM analysis in Figure 2f. Elemental mapping analysis revealed that the particles had different components: one was magnesium (Figure 3b), and the other was fluoride (Figure 3c). Well-distributed color intensities of the magnesium and fluoride elements confirm that the particles consisted of MgF_2 compounds.

The above results indicate that the addition of the magnesium and fluoride sources affords the formation of a MgF_2 shell layer on the surface of the PS spheres. Heat treatment of the core–shell PS/MgF_2 particles instigated removal of the PS core without any influence on the elemental composition and crystal phase/pattern of the formed MgF_2. This is confirmed by the decrease in the carbon intensity in EDS analysis but the constant XRD patterns and EDS ratio intensities of the magnesium and fluoride elements of the samples before and after heat treatment. Physical observations by electron microscopes confirm that core removal subsequently results in the formation of hollow particles. The size of the cavity is comparable with that of the PS spherical core, indicating that the generated cavity is a replication of the PS sphere. Although a similar hollow formation has been widely reported, to the best of our knowledge, this is the first report on the formation of a MgF_2 layer on the surface of colloidal particles featuring a uniform topological structure under additive-free conditions.
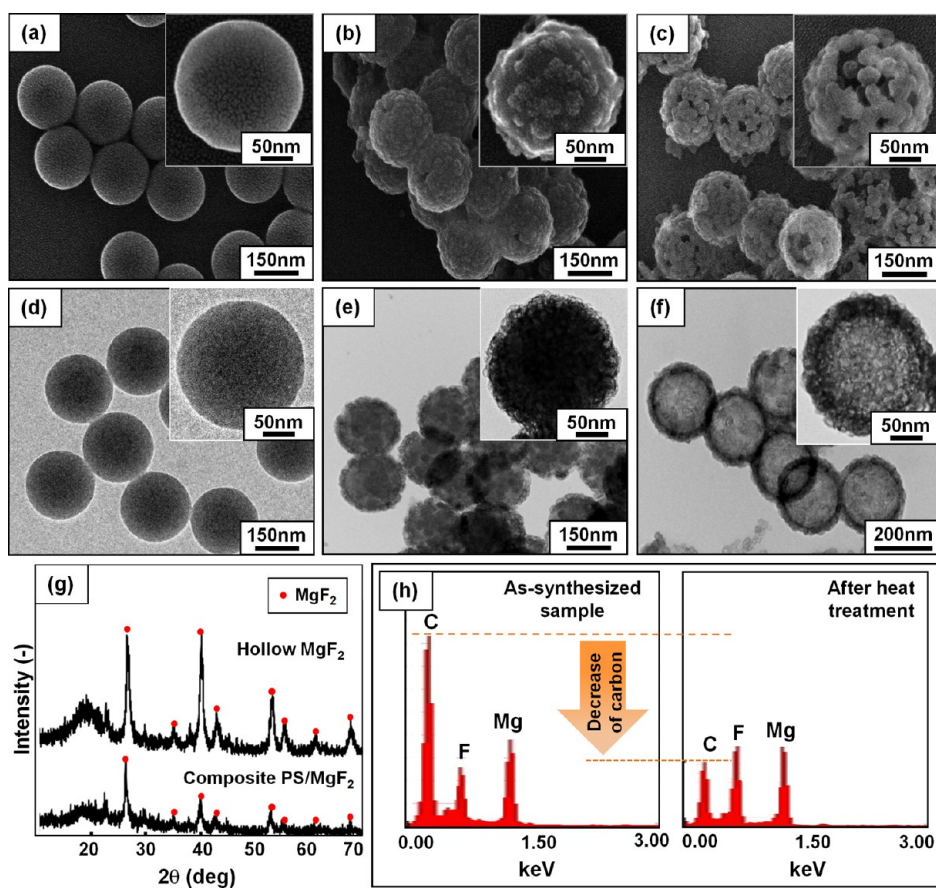
Figure 2. Physicochemical properties of the prepared particles. SEM images of the initial PS spheres (a), as-synthesized particles prior to heat treatment (b), and particles after heat treatment (c). Parts d–f correspond to the TEM images of samples shown in parts a–c, respectively. The insets show high-magnified images of corresponding particles. Parts g and h show XRD patterns and EDS analysis of the particles, respectively.
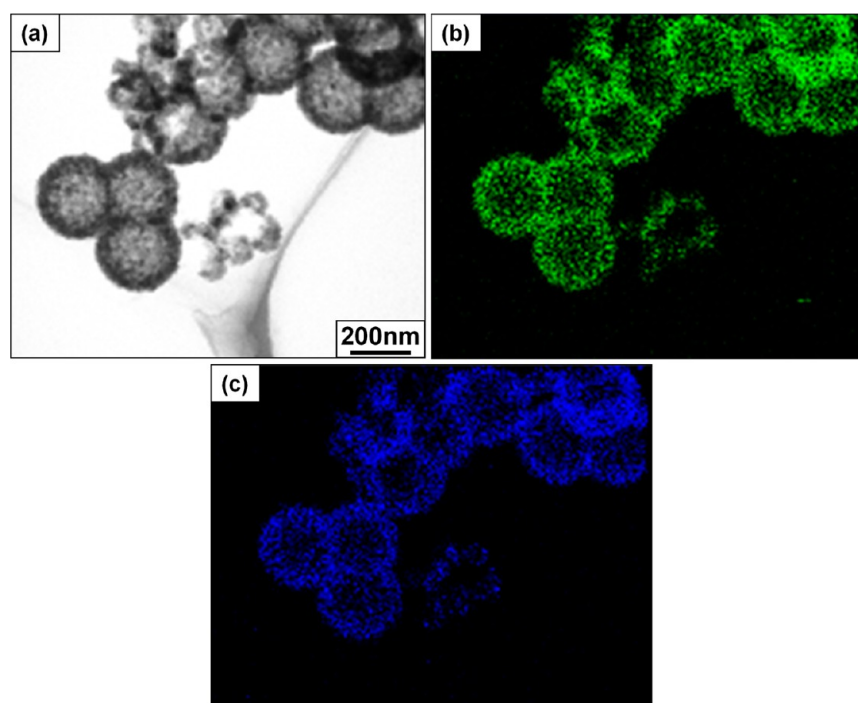

Figure 3. STEM (a) and elemental mapping analysis (b and c) of the particles after heat treatment. Parts b and c are magnesium and fluoride elemental mapping analysis, respectively.

4421

dx.doi.org/10.1021/am500139m | *ACS Appl. Mater. Interfaces* 2014, 6, 4418–4427

4.2. Influence of Synthesis Parameters Proposed in the Hypothesis To Control MgF$_2$ Formation and the Deposition Size for Creating Hollow Particles with Controllable Shell Structure. On the basis of the proposed model depicted in Figure 1, several parameters involve the selective deposition size and formation of the MgF$_2$ component on the surface of a PS core under additive-free conditions: reaction temperature and physicochemical properties of the PS core and MgF$_2$ components (i.e., surface charge, size, and composition). These are discussed as follows.

4.2.1. Effect of the Surface Charge of the Core and Shell Components. To achieve successful formation of the shell on the core surface, the core must be able to attract the shell component and provide space for subsequent deposition and shell growth.[7] A possible attraction mechanism for the present reaction, which is under additive-free conditions, is via electrostatic attraction phenomena.

To assess the MgF$_2$ coating, PS spheres with different surface charges were examined (Figure 4). To control the charge of the
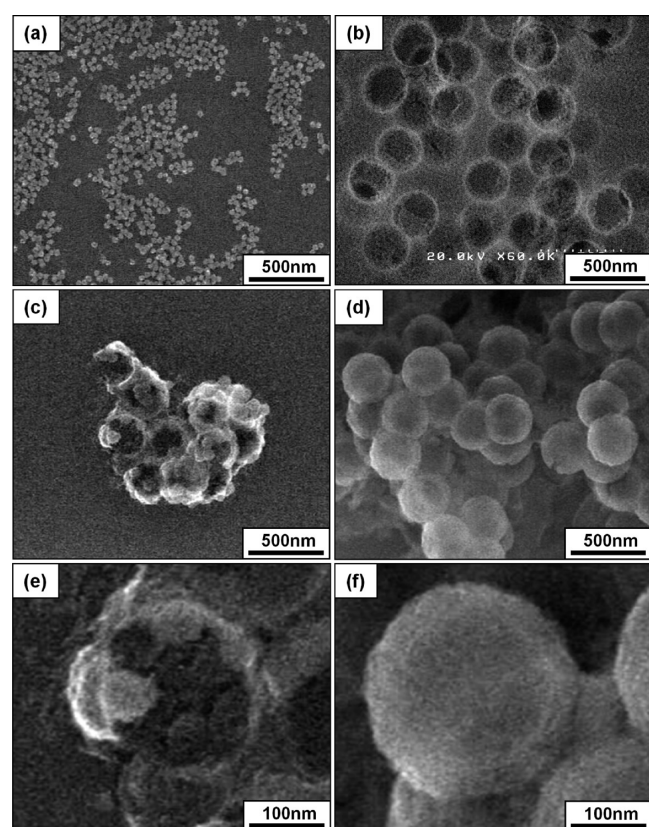
precursor generated particles with cavities of sizes comparable with those of the PS spheres (hole size of about 200 nm; Figure 4b−d). Different cavity configurations were obtained depending on the type of PS core. A porous filmlike structure was observed (Figure 4b) when cationic PS (prepared with 0.40 mg L^{-1} of AIBA) was used. In contrast, broken hollow particles (incomplete shell; Figure 4c) were obtained when anionic PS (prepared from 0.04 mg L^{-1} of KPS) was used. Increasing the KPS concentration to 0.40 mg L^{-1} afforded the generation of hollow spherical particles (Figure 4d).

To confirm the structure of the shell in samples shown in Figure 4c,d, high-magnified SEM images are shown in Figure 4e,f. The result shows that when using anionic PS with 0.04 mg L^{-1} of KPS, the shell consisted of compact multisized nanoparticles (Figure 4e). This result was different from the shell that was prepared using 0.40 mg L^{-1} of KPS (the shell consisted of a dense structure, shown in Figure 4f).

The ζ surface charge analysis of the particles is shown in Figure 5. The ζ potential value of MgF$_2$ nanoparticles was +33.90 mV.
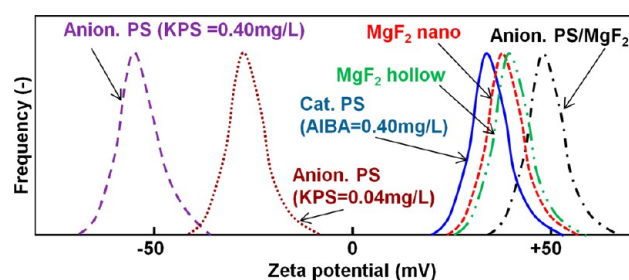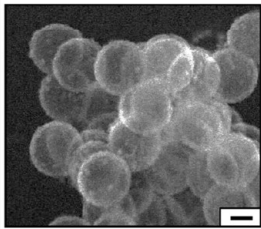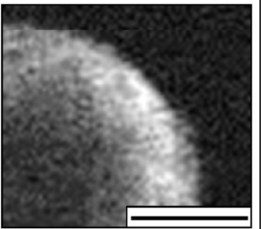

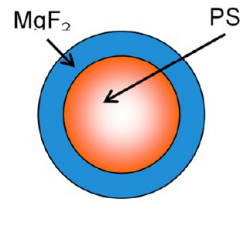**Figure 4.** SEM images of samples prepared from the precursor in the absence of a PS core (a) and with different PS core charges (b−d). Parts b−d are samples prepared with cationic PS (0.40 mg L^{-1} of AIBA), anionic PS (0.04 mg L^{-1} of KPS), and anionic PS (0.40 mg L^{-1} of KPS), respectively. Parts e and f are the high-magnified SEM images of samples in parts c and d, respectively.
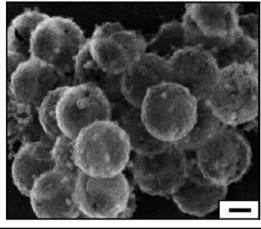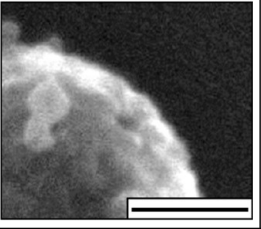
Figure 5. ζ potential analysis results of the prepared particles (i.e., PS, MgF$_2$ nano, and MgF$_2$ hollow).

The ζ values for cationic PS (0.40 mg L^{-1} of AIBA), anionic PS (0.04 mg L^{-1} of KPS), and anionic PS (0.40 mg L^{-1} of KPS) were +38.00, −54.90, and −25.00 mV, respectively. The ζ potential values of cationic PS/MgF$_2$ and hollow MgF$_2$ (prepared from anionic PS with 0.40 mg L^{-1} of KPS) were +48.10 and +38.7 mV, respectively.
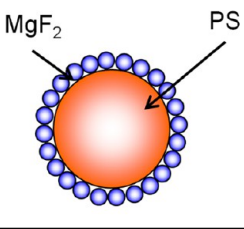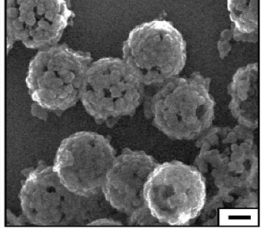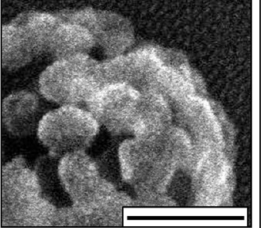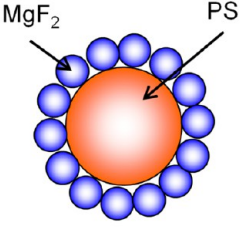
The above experimental results confirm that attraction between the oppositely charged MgF$_2$ and PS core affords a successful coating process. In simplification, because the reaction of MgCl$_2$ and NH$_4$F creates MgF$_2$ with a positive ζ charge, negatively charged PS spheres are essential toward the successful formation of hollow particles. Owing to the attractive forces of attraction, MgF$_2$ self-assembles and grows on the PS surface until complete PS surface coverage is achieved, as confirmed by the positive surface charge of the resulting core−shell and hollow samples. In addition to the opposite charge requirement of the PS core and MgF$_2$, the magnitude of the surface charge of the PS spheres is crucial because it influences the ability of the PS spheres to attract the MgF$_2$ component. Reduced surface charge values result in nonoptimal adsorption and growth of MgF$_2$ on the PS surface, producing a MgF$_2$ shell that is prone to collapse following heat treatment.

4.2.2. Effect of the Reaction Temperature. The influence of the reaction temperature on the morphology of the prepared particles, associated with illustrative models of the MgF$_2$ shell arrangement, is presented in Table 1. A low synthesis temperature (i.e., 30 °C) allows the formation of hollow particles with a smooth shell (sample A). Increasing the reaction temperature to 45 °C generates particles with a papillary surface (sample B). The size of the papilla nanoparticles is about 20 nm.

PS core, different types of initiators (i.e., KPS and AIBA) at various concentrations were used during the synthesis of the PS spheres. When the precursor with no additional PS core component was used alone in the synthetic procedure, nanoparticles with sizes of about 10 nm were created (Figure 4a), confirming the successful conversion of magnesium and fluoride sources into MgF$_2$. However, the addition of PS spheres in the

Table 1. SEM Images and Schematic Models of Particles Prepared at Various Reaction Temperatures: (A) 30, (B) 45, and (C) 75 °C[a]

Sample	Analysis results		
	Low-magnified SEM image	High-magnified SEM image	Model
A			
B			
C			

[a]Samples were prepared using a PS diameter of 250 nm. Scale bars are 100 nm.

A further temperature increase to 70 °C produces raspberry-like hollow particles (sample C). Larger papilla nanoparticles (about 40 nm) were observed, and some particles featured cavities in the shell.

TEM analysis of the particles prepared at the different temperatures studied confirmed the hollow structure of the particles (Figure 6). Different shell morphologies were observed depending on the temperature used during the coating process. Lower reaction temperatures produced hollow particles with a smooth shell (Figure 6a,b), whereas elevated reaction temperatures generated hollow particles with a raspberry-like shell morphology (Figure 6c,d). The shell comprised aggregated small shell components, as indicated by the protruding surface morphology.

The change in the shell morphology from dense to papillary confirms that the coating mechanism depends on deposition of the MgF_2 component size on the PS surface. Because the growth rate of MgF_2 is dependent on the temperature, the latter parameter effectively determines what size of MgF_2 can be deposited. A low-temperature process allows slow MgF_2 formation. The as-formed MgF_2 tends to be captured by the PS core, generating final particles with a smooth shell. This phenomenon can be described by routes R1−R3 in Figure 1. In contrast, elevated temperatures allow rapid MgF_2 formation, thereby promoting selective growth of the individually formed MgF_2 particles over deposition onto the PS surface in the earlier stages of the synthesis. Consequently, this generates a MgF_2 shell consisting of nanoparticles (as depicted in routes R4 and R5 in Figure 1).
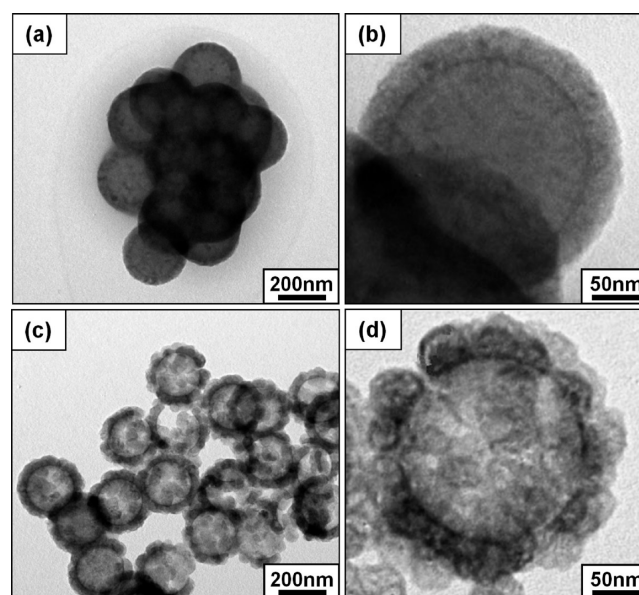

Figure 6. TEM images of particles prepared at different temperatures. Parts a and b were prepared at 30 °C, whereas parts c and d were at 75 °C. Images b and d are high-magnified TEM images of images a and c, respectively.

As mentioned above, elevated reaction temperatures are effective to generate hollow particles with papillary structures (Figure 7a). However, the hollow particles with larger size of
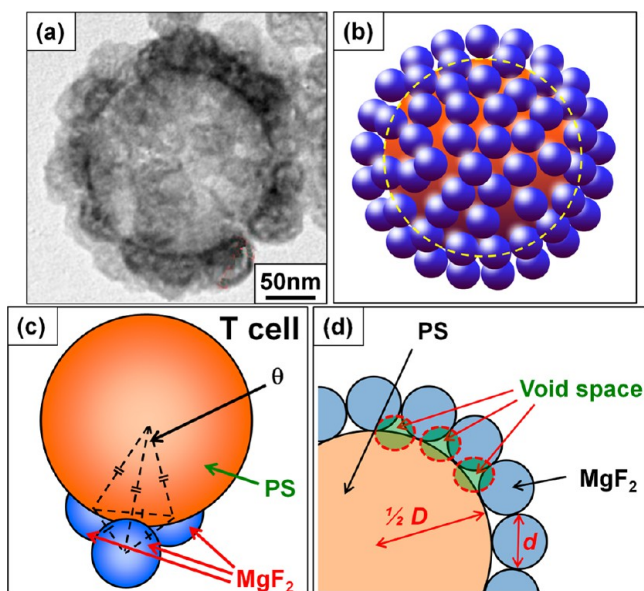
Figure 7. SEM image of a hollow MgF$_2$ particle with a papilla-structured shell (a), a three-dimensional representation of the hollow particle with a papilla-structured shell (b), and parameters used in the calculation (c and d). Part c is the tetragonal cell illustration model (T cell), and part d is the two-dimensional illustration model.

papilla have some fractures and holes. The reason of the formation of fractures can be described in the following. When deposited nanoparticles are too large, the available space on the PS surface for depositing MgF$_2$ is not large enough to contain multiple MgF$_2$ nanoparticles with a hexagonal structure. Frustration of MgF$_2$ nanoparticles arranged on the surface happens, resulting in the formation of incomplete shells. These observations can be explained using simple geometrical analysis (Figure 7b−d). Taking into account the arrangement of three adjacent MgF$_2$ nanoparticles on a PS core to form tetrahedral structures, the maximum size d of a MgF$_2$ nanoparticle that is able to fit on the surface of the PS particle with diameter D is determined by

$$d = [1 − \cos(\theta/2)/\cos(\theta/2)]D \qquad (3)$$

where θ denotes the angle between the three adjacent MgF$_2$ nanoparticles and the PS core. To obtain the minimum void space (void space less than 5%), eq 3 can be redefined as $d \approx 0.16D$. This value is crucial to determining the maximum size of the MgF$_2$ nanoparticle to be deposited on an available area on the surface of the PS core with a highly ordered arrangement. For instance, PS spheres with diameters of 200 nm require MgF$_2$ nanoparticles with sizes of at most 32 nm. Larger size MgF$_2$ nanoparticles induce distortion and alter the arrangement of other deposited MgF$_2$, resulting in a collapse of the highly ordered shell structure (having some cracks/holes in the shell).

4.2.3. Effect of the Magnesium and Fluoride Source Composition. The effect of the magnesium and fluoride composition on the formation of MgF$_2$ on the surface of PS is herein discussed in Figure 8. Parts a−f of Figure 8 show the SEM images of the resulting MgF$_2$ particles, following heat treatment at 500 °C, prepared using MgCl$_2$/NH$_4$F molar ratios of 1.00, 2.30, 3.30, 4.00, and 5.00, respectively. A MgCl$_2$/NH$_4$F molar ratio of 1.00 failed to generate a successful coating, as indicated by the presence of free non-hollow MgF$_2$ nanoparticles (Figure 8a). Larger MgF$_2$ particles (as indicated by the yellow arrows)

and some cavities, likely due to PS removal (as indicated by the red encircled areas), were also observed. However, different results were obtained when using a higher ratio. Some hollow structures were apparent as the ratio in the initial precursor increased (between 2.00 and 3.30; Figure 8b). Although an incomplete shell structure was found, this result indicated that MgF$_2$ started to coat PS. A further increase in the molar ratio (between 3.30 and 4.00) afforded the successful production of hollow particles (Figure 8c,d). However, higher molar ratios (i.e., 5.00) resulted in the additional formation of nanoparticles, as indicated by the red arrow in Figure 8e.

TEM analysis of the samples discussed in Figure 8c,d confirmed the hollow structure of the prepared particles (Figure 8f,g). The shell thickness decreased (from 22 to 11 nm) with increasing molar ratios, suggesting possible control of the shell thickness by regulating the ratio of the magnesium and fluoride sources in the precursor.

The molar ratio that is influenced by the amount of anion (i.e., fluoride ion) in the solution is known to influence the rate of particle formation.[9] Because the anion tends to actively attack and be adsorbed onto the inorganic ion (i.e., magnesium ion), a decrease in the ratio (effectively increasing the amount of anion) enables rapid evolution of the particles (nucleation and growth), subsequently influencing the coating process. Thus, controlling the ratio is crucial to regulating the rates of MgF$_2$ formation and subsequent deposition on the PS surface. Adequate MgCl$_2$/ NH$_4$F ratios afford deposition of MgF$_2$ and subsequent self-assembly onto the PS surface, thereby generating hollow particles with a good shell structure (Figure 8c,d,f,g). In contrast, deviation from optimum molar ratios results in a failure of the coating process. Considerably, low molar ratios promote rapid particle formation to monomers that preferentially grow over being adsorbed onto the PS core. This leads to the alternative formation of free MgF$_2$ nanoparticles in the final product (Figure 8a). Excessively high molar ratios result in overinteraction among the reactant molecules, instigating excessive nuclei formation. Because the availability of the active reactant and monomer is limited, the growth of MgF$_2$ both in the solution (as an individual particle) and on the surface of PS (as a deposited component) is delayed. This leads to the development of a brittle shell that fractures or the gradual enlargement of cracks. Thus, both free nanoparticles and hollow particles are obtained (Figure 8e).

4.2.4. Effect of the Core Diameter. To confirm that our coating method is effective for various core sizes, the present coating method was also examined using PS cores of various diameters (Figure 9). Parts a-c of Figure 9 show the TEM images of the resulting hollow particles prepared with different PS diameters, whereas Figure 9d shows the relationship between the PS diameter, resulting hollow particle outer diameter, and shell thickness. All processes were conducted under an optimum MgCl$_2$/NH$_4$F molar ratio of 4.00 and a temperature of 45 °C to examine the sole influence of the PS core diameter. Ferret analysis of the TEM images showed that the shell thicknesses of the samples prepared with PS diameters of 332, 198, and 106 nm were about 10, 10, and 9 nm, respectively. Hollow structures were obtained at all PS cores studied because all shell thicknesses were below the maximum allowed shell thickness (as calculated by eq 3). Also, because of the similar coating process conditions, the shell thicknesses of all studied samples were comparable. These results confirm that our MgF$_2$ coating method is applicable to cores with defined shape and various diameters; also the shape and size of the resulting hollow MgF$_2$ are influenced by the core template.
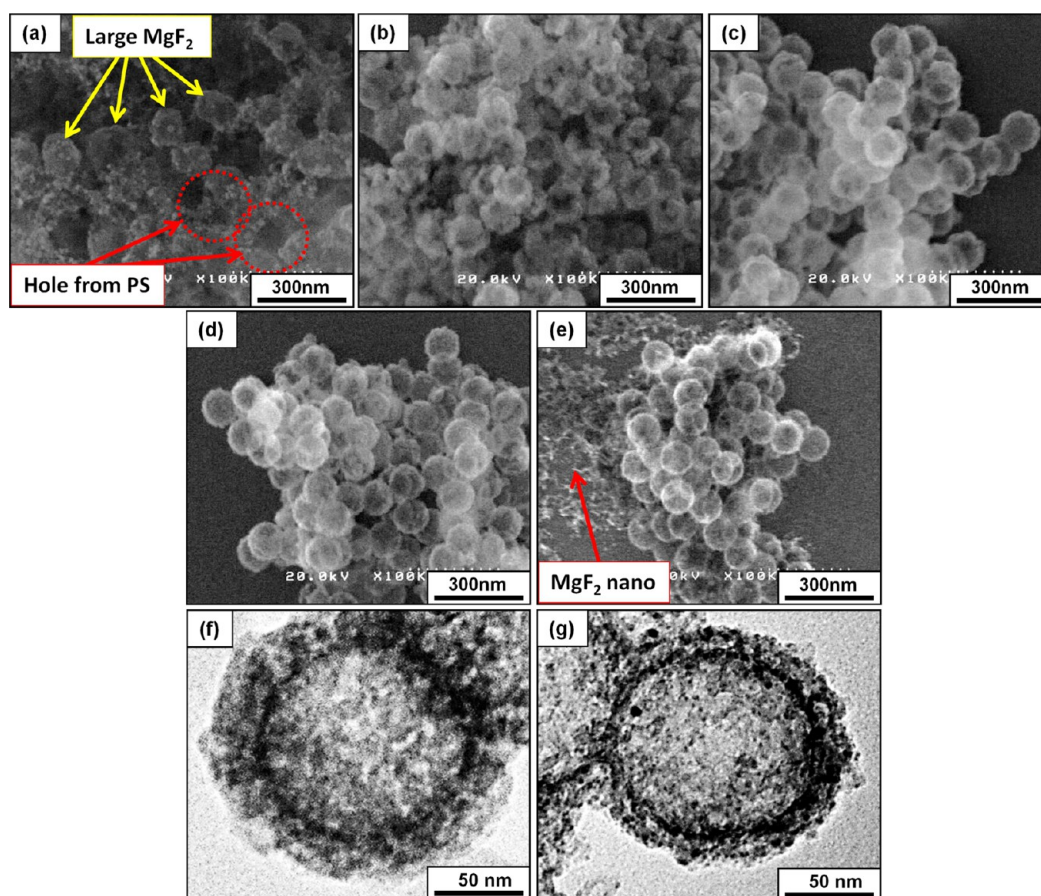
Figure 8. SEM images of particles prepared at various $MgCl_2/NH_4F$ molar ratios: (a) 1.00; (b) 2.30; (c) 3.30; (d) 4.00; (e) 5.00. Parts f and g are TEM images of the samples shown in images c and d, respectively. Samples were prepared using a PS diameter of 100 nm.
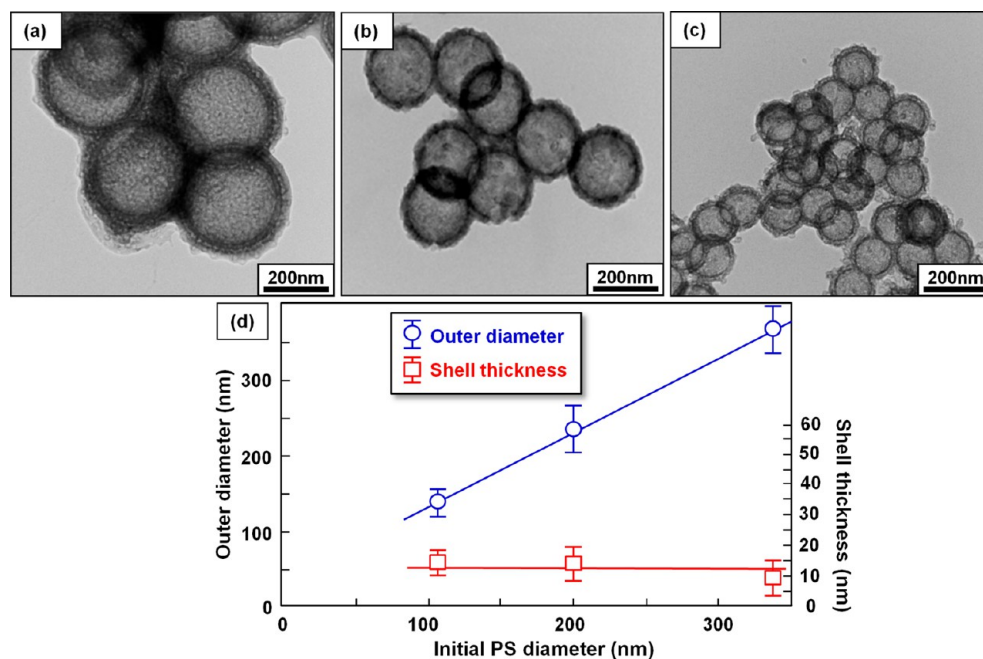

Figure 9. TEM images of particles prepared at various PS core diameters: (a) 332, (b) 198, and (c) 106 nm. Part d is the relationship between the average hollow particle outer diameter and shell thickness at a given initial PS diameter.

4.3. Proposed Formation Mechanism of the Hollow Particles.

The formation of hollow MgF_2 particles with controllable shell thickness and morphology was successfully achieved by careful regulation of the interaction and reaction between the PS core and MgF_2 component (Figure 10). As mentioned earlier, $MgCl_2$ and NH_4F are quickly converted to
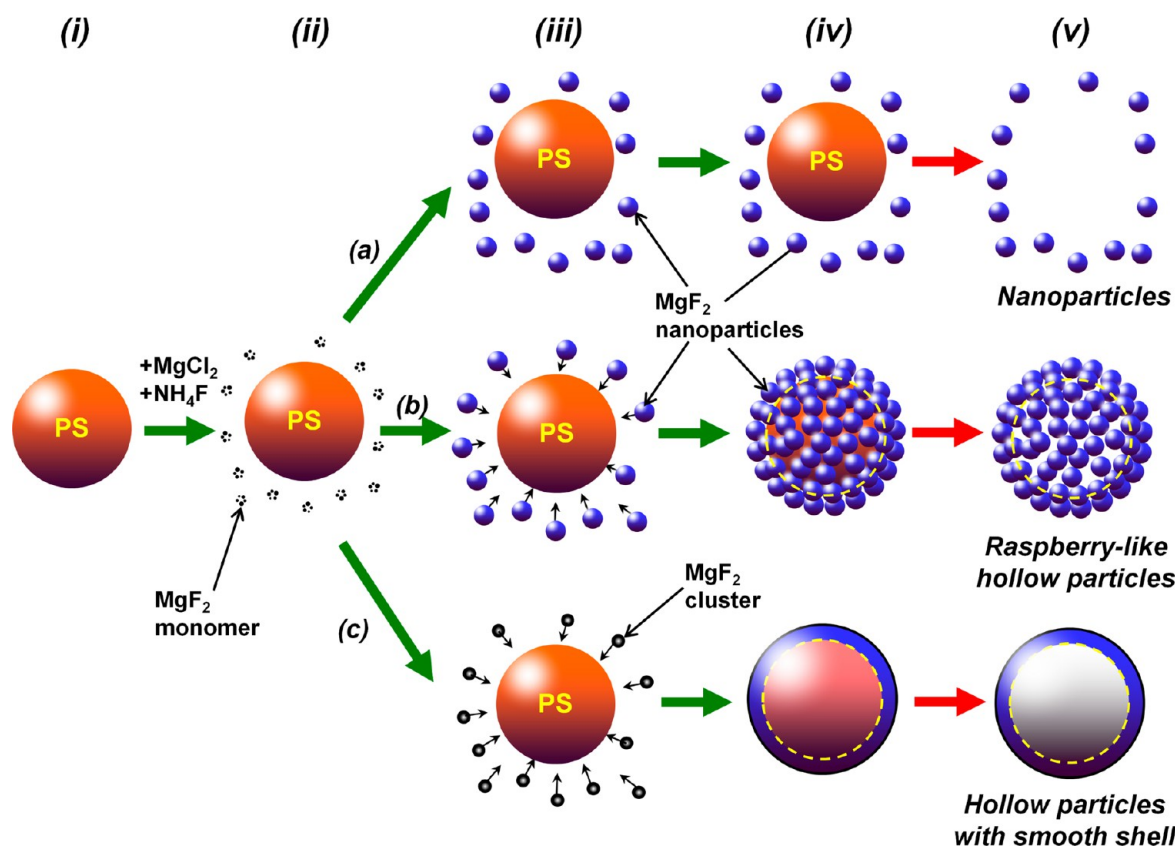
Figure 10. Schematic representation of the formation of MgF_2 on the surface of PS. Detailed formation steps are described as follows: (i) preparation of a PS core with a well-defined morphology; (ii) formation of MgF_2 monomers following the addition of $MgCl_2$ and NH_4F; (iii) growth and electrostatic attraction of MgF_2 to the surface of PS; (iv) deposition of MgF_2 on the surface of PS, followed by further growth, generating core−shell PS/MgF_2 particles; (v) removal of the PS core via heat treatment, generating the final product. The development of hollow particles is dependent on the success of MgF_2 deposition following monomer formation. Route a: unsuccessful attraction of MgF_2 onto the surface of PS results in non-hollow nanoparticles. Route b: successful attraction of MgF_2, provided the rate of MgF_2 growth is faster than that of MgF_2 deposition on the surface of PS, produces raspberry-like hollow particles. Route c: successful attraction of MgF_2, provided the rate of MgF_2 growth is slower than that of MgF_2 deposition on the surface of PS, generates hollow particles with a smooth shell.

form a MgF_2 monomer (Figure 10i,ii). The monomer then undergoes nucleation and growth upon consumption of other MgF_2 monomers, forming clusters. The cluster is a minimum requirement for MgF_2 to be attracted by the surface of the PS core via electrostatic forces (Figure 10iii). The cluster can participate in three possible routes: (1) the cluster grows independently and is not influenced by the electrostatic attractive force exerted by the PS core (Figure 10, route a); (2) the cluster is attracted by the PS core provided that the rate of MgF_2 formation is faster than that of MgF_2 deposition on the PS surface (Figure 10, route b); (3) the cluster is attracted by the PS core provided that the rate of MgF_2 formation is slower than that of MgF_2 deposition on the PS surface (Figure 10, route c). Upon attraction and deposition of the MgF_2 components on the PS surface, the deposited components self-assemble and grow into a MgF_2 shell (Figure 10iv). Finally, following core template removal (Figure 10v), three types of particles are created: free nanoparticles, raspberry-like hollow particles, and hollow particles with a smooth shell.

On the basis of the experimental results, the adopted synthesis route depends on the parameters used during the coating process. Route a proceeds when PS spheres with a positive ζ surface charge are used, whereas routes b and c are achieved when PS spheres with a negative ζ surface charge are employed. In the cases of routes b and c, both routes can be tuned accordingly by controlling the reaction temperature and reactant composition. A high-temperature process allows the formation of raspberry-like hollow particles via route b, whereas a low-temperature process affords the formation of hollow particles with a smooth shell via route c. Additionally, modulation of the reactant composition enables the formation of hollow particles with different shell thicknesses.

5. CONCLUSIONS

Control of the shell structural properties of hollow particles was investigated experimentally, and the results were qualitatively explained using the available theory. Experimental results showed that, by control of the characteristics of MgF_2 deposition and formation on the surface of the PS core, a versatile synthesis strategy for efficient and independent control of the shell structural properties [i.e., thickness (8−25 nm) and morphology (dense and raspberry)] and cavity diameter (100−350 nm) of hollow MgF_2 particles was successfully developed. To achieve control of the characteristics of MgF_2 deposition and formation, we involved the regulation of various synthesis parameters (i.e., reaction temperature and charge, interaction, size, and composition of the core and shell components). Because, to the best of our knowledge, the present contribution is the first to address the controlled formation of a shell component on a core surface that is controlled by the synthesis parameters, further development in the present architecturally engineered synthesis

can significantly increase the possibilities of creating new and more varied properties for application explorations. Specifically, understanding how to tailor the formation of shells with various structures (both thickness and morphology) is a prospective for various applications, such as advanced lens synthesis, because control of this structure has a correlation with controlling the final material properties, such as the refractive index.

■ AUTHOR INFORMATION

Corresponding Author

*E-mail: ogit@hiroshima-u.ac.jp. Tel.: +81-82-424-7850.

Notes

The authors declare no competing financial interest.

■ REFERENCES

(1) Zhang, Q.; Wang, W.; Goebl, J.; Yin, Y. Self-templated Synthesis of Hollow Nanostructures. *Nano Today* **2009**, *4*, 494−507.

(2) Wang, A.-J.; Lu, Y.-P.; Sun, R.-X. Recent Progress on the Fabrication of Hollow Microspheres. *Mater. Sci. Eng., A* **2007**, *460*, 1−6.

(3) Lai, X.; Halpert, J. E.; Wang, D. Recent Advances in Micro-/nano-structured Hollow Spheres for Energy Applications: From Simple to Complex Systems. *Energy Environ. Sci.* **2012**, *5*, 5604−5618.

(4) Nandiyanto, A. B. D.; Akane, Y.; Ogi, T.; Okuyama, K. Mesopore-Free Hollow Silica Particles with Controllable Diameter and Shell Thickness via Additive-Free Synthesis. *Langmuir* **2012**, *28*, 8616−8624.

(5) Nandiyanto, A. B. D.; Suhendi, A.; Arutanti, O.; Ogi, T.; Okuyama, K. Influences of Surface Charge, Size, and Concentration of Colloidal Nanoparticles on Fabrication of Self-Organized Porous Silica in Film and Particle Forms. *Langmuir* **2013**, *29*, 6262−6270.

(6) Nandiyanto, A. B. D.; Kim, S.-G.; Iskandar, F.; Okuyama, K. Synthesis of Spherical Mesoporous Silica Nanoparticles with Nanometer-size Controllable Pores and Outer Diameters. *Microporous Mesoporous Mater.* **2009**, *120*, 447−453.

(7) Nandiyanto, A. B. D.; Iwaki, T.; Ogi, T.; Okuyama, K. Mesopore-free Silica Shell with Nanometer-scale Thickness-controllable on Cationic Polystyrene Core. *J. Colloid Interface Sci.* **2013**, *389*, 134−146.

(8) Nandiyanto, A. B. D.; Suhendi, A.; Ogi, T.; Iwaki, T.; Okuyama, K. Synthesis of Additive-free Cationic Polystyrene Particles with Controllable Size for Hollow Template Applications. *Colloid Surf., A* **2012**, *396*, 96−105.

(9) Nandiyanto, A. B. D.; Iskandar, F.; Ogi, T.; Okuyama, K. Nanometer to Submicrometer Magnesium Fluoride Particles with Controllable Morphology. *Langmuir* **2010**, *26*, 12260−12266.

(10) Nandiyanto, A. B. D.; Ogi, T.; Okuyama, K. Doughnut Magnesium Fluoride Nanoparticles Prepared by an Electron-beam Irradiation Method. *J. Nanopart. Res.* **2012**, *14*, 1182.

(11) Kemnitz, E.; Wuttke, S.; Coman, S. M. Tailor-Made MgF₂-Based Catalysts by Sol−Gel Synthesis. *Eur. J. Inorg. Chem.* **2011**, *2011*, 4773−4794.

(12) Gibson, U.; Kennemore, C., III. Ion-assisted Deposition of MgF₂ at Ambient Temperatures. *Thin Solid Films* **1985**, *124*, 27−33.

(13) Fujihara, S.; Tada, M.; Kimura, T. Preparation and Characterization of MgF₂ Thin Film by a Trifluoroacetic Acid Method. *Thin Solid Films* **1997**, *304*, 252−255.

(14) Tada, M.; Fujihara, S.; Kimura, T. Sol−gel Processing and Characterization of Alkaline Earth and Rare-earth Fluoride Thin Films. *J. Mater. Res.* **1999**, *14*, 1610−1616.

(15) Perales, F.; Herrero, J.; Jaque, D.; De las Heras, C. Improvement of MgF₂ Thin Coating Films for Laser Applications. *Opt. Mater.* **2007**, *29*, 783−787.

(16) Krüger, H.; Kemnitz, E.; Hertwig, A.; Beck, U. Transparent MgF₂-films by Sol−gel Coating: Synthesis and Optical Properties. *Thin Solid Films* **2008**, *516*, 4175−4177.

(17) Noack, J.; Scheurell, K.; Kemnitz, E.; Garcia-Juan, P.; Rau, H.; Lacroix, M.; Eicher, J.; Lintner, B.; Sontheimer, T.; Hofmann, T. MgF₂ Antireflective Coatings by Sol−gel Processing: Film Preparation and Thermal Densification. *J. Mater. Chem.* **2012**, *22*, 18535−18541.

(18) Cao, M.; Wang, Y.; Qi, Y.; Guo, C.; Hu, C. Synthesis and Characterization of MgF₂ and KMgF₃ Nanorods. *J. Solid State Chem.* **2004**, *177*, 2205−2209.

(19) Hsu, W. P.; Zhong, Q.; Matijević, E. The formation of uniform colloidal particles of magnesium fluoride and sodium magnesium fluoride. *J. Colloid Interface Sci.* **1996**, *181*, 142−148.

(20) Krishna Murthy, J.; Groß, U.; Rüdiger, S.; Kemnitz, E.; Winfield, J. M. Sol−gel-fluorination Synthesis of Amorphous Magnesium Fluoride. *J. Solid State Chem.* **2006**, *179*, 739−746.

(21) Wuttke, S.; Scholz, G.; Rüdiger, S.; Kemnitz, E. Variation of Sol−gel Synthesis Parameters and Their Consequence for the Surface Area and Structure of Magnesium Fluoride. *J. Mater. Chem.* **2007**, *17*, 4980−4988.

(22) Sevonkaev, I.; Matijevic, E. Formation of Magnesium Fluoride Particles of Different Morphologies. *Langmuir* **2009**, *25*, 10534−10539.

(23) Lellouche, J.; Kahana, E.; Elias, S.; Gedanken, A.; Banin, E. Antibiofilm Activity of Nanosized Magnesium Fluoride. *Biomaterials* **2009**, *30*, 5969−5978.

(24) Saberi, A.; Negahdari, Z.; Bouazza, S.; Willert-Porada, M. Synthesis and Characterization of Crystalline Nanosized MgF₂ Powder via Microemulsion Route. *J. Fluorine Chem.* **2010**, *131*, 1353−1355.

(25) Grosso, D.; Boissiere, C.; Sanchez, C. Ultralow-dielectric-constant Optical Thin Films Built from Magnesium Oxyfluoride Vesicle-like Hollow Nanoparticles. *Nat. Mater.* **2007**, *6*, 572−575.

(26) Sugimoto, T. *Monodispersed Particles*; Elsevier: Amsterdam, The Netherlands, 2001.

(27) Mullins, W. W.; Sekerka, R. Morphological Stability of a Particle Growing by Diffusion or Heat Flow. *J. Appl. Phys.* **1963**, *34*, 323−329.

(28) Kashchiev, D. On the Relation between Nucleation Work, Nucleus Size, and Nucleation Rate. *J. Chem. Phys.* **1982**, *76*, 5098.

(29) Wang, B.; Deng, L.; Wang, Y. Competition between Attraction and Diffusion in Nanoscale Non-equilibrium Aggregation. *Sci. China: Phys. Mech. Astron.* **2012**, *55*, 2237−2243.